Science Advances
AAAS

Manuscript Template

FRONT MATTER

Title

- Full title: CRISPR/Cas9-mediated therapeutic editing of *Rpe65* ameliorates the disease phenotypes in a mouse model of Leber congenital amaurosis
- Short title: Therapeutic *Rpe65* editing by CRISPR/Cas9

Authors

Dong Hyun Jo,[1†] Dong Woo Song,[2†] Chang Sik Cho,[1] Un Gi Kim,[2] Kyu Jun Lee,[2] Kihwang Lee,[3] Sung Wook Park,[1] Daesik Kim,[4] Jin Hyoung Kim,[1] Jin-Soo Kim,[4] Seokjoong Kim,[2] Jeong Hun Kim,[1,5,6*] and Jungmin Lee[2,7*]

Affiliations

[1]Fight against Angiogenesis-Related Blindness (FARB) Laboratory, Clinical Research Institute, Seoul National University Hospital, Seoul, Republic of Korea.
[2]ToolGen, Inc., Seoul, Republic of Korea.
[3]Department of Ophthalmology, Ajou University School of Medicine, Suwon, Republic of Korea.
[4]Center for Genome Engineering, Institute for Basic Science (IBS), Seoul, Republic of Korea.
[5]Department of Biomedical Sciences, Seoul National University College of Medicine, Seoul, Republic of Korea.
[6]Department of Ophthalmology, Seoul National University College of Medicine, Seoul, Republic of Korea.
[7]Department of Life Science, Handong Global University, Pohang, Korea.

[†]These authors contributed equally to this paper.

Abstract

Leber congenital amaurosis (LCA), one of the leading causes of childhood-onset blindness without a cure, is caused by autosomal recessive mutations in several genes including *RPE65*. In this study, we performed CRISPR/Cas9-mediated therapeutic correction of a disease-associated nonsense mutation in *Rpe65* in *rd12* mice, a model of human LCA. Subretinal injection of adeno-associated virus carrying CRISPR/Cas9 and donor DNA resulted in >1% homology-directed repair (HDR) and ~1.6% deletion of the pathogenic stop codon in *Rpe65* in retinal pigment epithelial tissues of *rd12* mice. Our approach recovered a- and b-waves of electroretinograms to levels up to 21.2±4.1% and 39.8±3.2% of their wild-type counterparts in *rd12* mice upon bright stimuli after dark adaptation at 7 months after injection. There was no definite evidence of histologic perturbation or tumorigenesis during 7 months of observation. Collectively, we present the first therapeutic correction of an *Rpe65* nonsense mutation by HDR using CRISPR/Cas9, providing new insight for developing therapeutics for LCA.

MAIN TEXT

Introduction

Leber congenital amaurosis (LCA) is a hereditary retinal degenerative disease leading to childhood-onset blindness (*1*). Among the genes causing LCA, *CEP290*, *GUCY2D*, *CRB1* and *RPE65* are those most frequently mutated. In particular, about 6% of LCA cases are caused by mutations in RPE65 (*2*). To date, no substantial treatments or cures for LCA have been developed, except voretigene neparvovec (Luxturna, Spark Therapeutics) approved by the Food and Drug Administration (FDA) in the United States. This approach is based on *RPE65* gene delivery by adeno-associated virus (AAV) to the retina in patients who lack the functional RPE65 protein (*3-5*). Based on preclinical studies performed in *RPE65* null dogs (*6, 7*) and mice (*8, 9*), initial clinical trials tested the adverse events and therapeutic outcomes of AAV containing the human *RPE65* cDNA (*3-5*). Although normal vision was not achieved, these trials showed that subretinal injection of AAV had an acceptable local and systemic adverse event profile as well as improved visual function (*10*). Nevertheless, because gene therapy cannot totally correct the mutated sequence and it has limitation in the cargo size of the AAV (~4.8 kb) when AAV is used, there are still unmet needs in the gene therapy area for broader clinical application.

CRISPR/Cas9 is a genome editing tool that can lead to the insertion of genes or the deletion of mutations (*11-15*) by homology-directed repair (HDR) or by non-homologous end joining (NHEJ), respectively. Although the frequency of HDR is generally lower than that of NHEJ, the ability of HDR to correct pathogenic mutations permanently has great potential for curing various genetic disorders (*16-18*). For example, intravenously infused AAV expressing the Cas9 machinery and the donor DNA reversed the disease-causing mutation and rescued the disease phenotypes in two different mouse models of metabolic diseases (*16-18*).

In this context, we hypothesized that CRISPR/Cas9 could represent another therapy for LCA and tested therapeutic outcomes of CRISPR/Cas9-mediated HDR in *rd12* mice, a model of human LCA that bears a disease-associated premature stop codon in *Rpe65*. We utilized CRISPR/Cas9 technology to correct the nonsense mutation in this model, and found that HDR and in-frame NHEJ in response to CRISPR/Cas9-mediated DNA cleavage led to the recovery of retinal functions and protection from retinal degeneration. The results from this proof-of-concept study demonstrate the feasibility of our approach and imply that CRISPR/Cas9-mediated HDR could be expanded to other ophthalmologic diseases in which HDR might be needed.

Results

CRISPR/Cas9-medated editing of *Rpe65 in vitro*

To utilize CRISPR/Cas9 technology for treating LCA, we first screened single guide RNA (sgRNA) sequences targeting *Rpe65* exon 3 in the region that corresponds to the C-to-T nonsense mutation locus using mouse embryonic fibroblasts (MEFs) from *rd12* mice (**fig. S1A**). Of 9 potential candidates tested, the TS4 sgRNA was selected for further studies because it generated double strand break (DSB) at the nearest locus form the premature stop codon and resulted in highly efficient insertion or deletion (indel) rates as determined by targeted deep sequencing when transfected with SpCas9 protein as riboneucleoprotein

(RNP) complex (**fig. S1B**). Next, we examined the correction frequencies by HDR induced by the TS4 sgRNA and *Rpe65* donor in *rd12* MEFs. Synonymous mutations were introduced into the donor sequence to prevent cleavage of the donor itself or re-cleavage of the repaired *Rpe65* locus after correction (**Fig. 1A and F**). Single stranded oligodeoxynucleotide (ssODN) was used as a *Rpe65* donor and induced correction in a range of 3 to 6% (**Fig. 1B, C, and F**). Interestingly, when NHEJ was analyzed by deep sequencing, TS4 sgRNA-mediated indels were dominated by deletions, and approximately one fourth of the mutations corresponded to in-frame indels (**Fig. 1D and E**). Among the in-frame indels, one-codon deletions accounted for 5.6% of the total reads (**Fig. 1F**). Because the in-frame indels could result in the removal of the premature *Rpe65* stop codon from *rd12* mice, we suggest that NHEJ-mediated editing might also contribute to the therapeutic effects of CRISPR/Cas9. These data indicate that we identified an optimized sgRNA sequence for therapeutic, CRISPR/Cas9-mediated genome editing to treat LCA.

In vivo genome editing of *Rpe65* using the dual AAV system

To evaluate the therapeutic efficacy of CRISPR/Cas9-medated editing of the *Rpe65* nonsense mutation in a disease model, we changed one nucleotide in TS4 to design the TS4^{rd12} sgRNA, which perfectly matches the sequence of the *Rpe65* exon 3 mutation locus in *rd12* mice. All required editing components were incorporated into two separate AAVs (AAV-SpCas9 and AAV-TS4^{rd12} sgRNA-*Rpe65*-donor, hereafter referred to as AAV-TS4^{rd12}-donor) and *in vivo* delivery was carried out using the dual AAV system (**Fig. 2A**). We optimized the ratio of AAV components by varying their concentrations to obtain maximized genome editing results. A low dose (a total of $2x10^{10}$ vector genomes (vg)/eye) or high dose (a total of $2x10^{11}$ vg/eye) of AAVs were administered via subretinal injection into 3-week-old *rd12* mice. After 4 weeks of AAV treatment, the targeted region of *Rpe65* was analyzed by deep sequencing using cells from the retina and retinal pigment epithelium (RPE). Subretinal injection resulted in indel rates in the retina and RPE that reached ~20%, but that varied depending on various parameters **(Fig. 2B and C**). Low dose subretinal injection induced low and high indel rates in the retina and RPE, respectively. This result indicates that subretinal AAV administration is more efficient in the RPE versus the retina; this conclusion was further verified by the finding of a higher AAV copy number per diploid cell **(Fig. 2D and fig. S2)** in the RPE. Because a previous study showed that use of a high (10:1) ratio of sgRNAs and donor to Cas9 induced a further increase in the frequency of a correction in a mouse model of liver disease (*18*), an excessive amount of AAV-TS4^{rd12}-donor relative to AAV-SpCas9 (AAV-SpCas9:AAV-TS4^{rd12}-donor ratio of 0.1:1.9) was tested, but it resulted in a lower frequency of indels in both tissues after subretinal administration (**Fig. 2B and C**). Collectively, these data suggest that subretinal delivery is an efficient method of inducing *in vivo Rpe65* editing and that the Cas9 to sgRNA ratio is critical for optimized editing.

In vivo correction of the *Rpe65* mutation in *rd12* mice

Subsequently, we analyzed HDR events near the pathogenic C-to-T mutation in *Rpe65* in the retina and RPE after AAV treatment in *rd12* mice. HDR events were clearly observed in the RPE but not in the retina (**Fig. 2E**). Although indel frequencies were comparable between low dose and high dose AAV-treated RPE when a 1:1 ratio of AAV-SpCas9 to AAV-TS4-donor was used (**Fig. 2C**), HDR events were more frequent in the high dose AAV-treated group (high dose, 1.17±0.31%; low dose, 0.59±0.22%) (**Fig. 2E**) as similarly

observed in the CRISPR-mediated correction of the ornithine transcarbamylase gene in hepatocytes (*18*). Moreover, analysis of the HDR to indel ratio revealed that HDR events were approximately three times more frequent in the high dose-treated group (**Fig. 2F**). Successful HDR (1.01±0.38%) was also induced by the application of a 0.5:1.5 ratio of AAV-SpCas9 to AAV-TS4-donor (**Fig. 2E**). Importantly, it should be noted that most HDR events resulted in a precise correction of the T-to-C mutation, so that the resulting protein sequences were identical to that of wild-type Rpe65 (**Fig. 2H**). We additionally characterized NHEJ-mediated editing in the RPE and found that in-frame deletions occurred at a frequency of 3.83%; 1.61% were one-codon deletions that resulted in the removal of the premature stop codon in *rd12* mice (**Fig. 2G and H**). Interestingly, the 1-codon-Del-2 type (CGT-deletion) was also predicted as one of the top 3 end-joining categories (**table S1**) by inDelphi, the machine learning model that predicts SpCas9-mediated template-free genome editing (*19*). In addition, substantial in-frame editing was achieved in human *RPE65* with the use of various sgRNAs in HEK293 cells, suggesting the clinical potential of our approach (**fig. S3A-C**).

Recovery of retinal function induced by *Rpe65* correction in *rd12* mice

To investigate the therapeutic effects of HDR-mediated *Rpe65* gene correction in *rd12* mice, we performed electroretinography after dark adaptation at 6 weeks and 7 months after subretinal AAV injection (**Fig. 3A**). AAV treatment led to the recovery of Rpe65 expression in RPE cells at 6 weeks after injection (**Fig. 3B**). Furthermore, AAV treatment resulted in increased *Rpe65* gene expression in RPE cells at 7 months after injection (**Fig. 3C**). In electroretinography, *rd12* mice demonstrated severely attenuated dark-adapted light responses compared to age-matched normal C57BL/6 mice (*20*). In contrast, there were definite responses to bright stimuli (0 dB) by which both rod and cone responses are provoked after dark adaptation in the AAV-treated *rd12* mice at 6 weeks after the subretinal injection (**Fig. 3 D-F and fig. S4**), whereas there were no responses to dim stimuli (-25 dB) (**fig. S5**). The electrical responses were maintained up to 7 months after the initial injection (**Fig. 3G and H**). The estimated a- and b-wave amplitudes were 21.2±4.1% and 39.8±3.2% of those of normal C57BL/6 mice. These functional recoveries were accompanied by anatomical changes in which HDR-mediated *Rpe65* gene correction prevented the loss of neuronal cells in the outer nuclear layer of the retina in *rd12* mice (**Fig. 3I and J**).

Genome-wide off-target analysis of *Rpe65*-specific CRISPR/Cas9

To globally characterize potential off-target sites recognized by the TS4^{rd12} sgRNA, we performed Digenome-seq, a genome-wide unbiased off-target detection method (*21*), using genomic DNA from *rd12* mice. This analysis showed several potential off-target sites (**Fig. 4A**). We validated the 29 potential off-target sites with the highest Digenome-seq cleavage scores using targeted deep sequencing. Interestingly, 6 genomic loci were shown to be actively targeted by the TS4^{rd12} sgRNA in the retina of *rd12* mice (**Fig. 4B**), and these off-target sites were consistently found to be targeted in the RPE (**Fig. 4C**). All of the active off-target sites are located in intronic or intergenic regions (**table S2**). In subsequent off-target analysis for all 33 homologous sites that differed from the TS4^{rd12} sgRNA sequence by up to 3 nucleotides, no meaningful indel mutations were observed at the predicted genomic loci in AAV-treated *rd12* mice (**fig. S6**). In addition, there was no definitive evidence of histologic perturbation or tumorigenesis for 7 months in these mice (**Fig. 4D)**.

Discussion

In this study, we deployed CRISPR/Cas9-mediated HDR as a new treatment for LCA. We showed that dual AAV-mediated delivery of CRISPR/Cas9 and an *Rpe65* donor sequence can lead to the correction of a disease-causing mutation in *Rpe65* and an improvement in retinal function in a mouse model of LCA. In addition to this improvement, our study showed a level of functional recovery exceeding the measured gene correction level. The results are provocative because in post-mitotic cells, HDR events are generally known as rare. However, our observations are supported by recent studies showing CRISPR/Cas9-mediated HDR events in post-mitotic neurons (*22*) and muscles (*23*)**.** Our results are also supported by previous studies in which CRISPR/Cas9 treatment for certain autosomal recessive diseases, such as Duchenne muscular dystrophy (*23*) and retinitis pigmentosa (*24*), resulted in functional improvement beyond the level expected from the gene correction frequency. Together, these results suggest that HDR can be activated in these post-mitotic cells, and that therapeutic outcomes exceeding that expected from the editing level could be achieved in some cases.

Gene therapy works by using viruses as a means of overexpressing wild-type copies of defective, disease-associated genes. For instance, Luxturna, the FDA-approved gene therapy for LCA, uses AAV2 to express functional RPE65 to replace the mutant, LCA-associated RPE65 protein. Different types of viruses, such as lentivirus and retrovirus, can also be used for gene therapy, but AAV is clinically validated (*3-5, 25, 26*). Although AAV is very attractive for gene therapy because it does not integrate into the host genome, its limited cargo packaging capability hinders its application in many cases. Therefore, for some ocular diseases such as Stargardt disease or Usher syndrome that require the delivery of large DNA fragments, our approach using CRISPR/Cas9-mediated HDR could be suitable therapeutically. In addition, because the desired wild-type sequence can be introduced at the genomic site where the gene should exist replacing the mutant sequence by HDR, the HDR-corrected cells can express the introduced genes at the endogenous level. In this study, CRISPR/Cas9 was randomly introduced into the eye by subretinal injection in *rd12* mice because mice lack a macula, the center and core of vision in humans. The injection resulted in a frequency of gene correction of nearly 3% by HDR and in-frame NHEJ **(Fig. 2E, F, and H),** and led to significant improvement in electroretinography measurements **(Fig. 3 D-H**). We expect that these results in mice can be further improved in human LCA patients because ophthalmologists can selectively perform subretinal injection near the macular area, enabling focused editing around this structure to achieve even more restoration of vision.

The deep sequencing in our study provides a detailed description of the types of indels generated as well as the extent of off-target mutations produced, which was extensive. Although the active off-target sites that we detected were within intronic or intergenic regions, this level of off-target effects could undermine the therapeutic potential of our approach using CRISPR/Cas9-mediated genome editing. As the first study using CRISPR/Cas9 to treat LCA, we utilized wild type SpCas9, the conventional and most commonly used form of Cas9. To reduce the frequency of off-target mutations, high fidelity versions of Cas9 (HFCas9, eCas9, HypaCas9 (*27*), SniperCas9 (*28*), or self-targeting AAV (*29*), or inducible-editing (*30*) could be tried as alternatives. In fact, we tested SniperCas9 (*28*), a high-fidelity version of SpCas9 that was developed by our group in the C2C12 cell line. We found that SniperCas9 was associated with a significant reduction in indel frequencies at the off-target sites recognized by SpCas9 **(fig. S7)**. In

addition, SniperCas9 showed comparable activity against the mRosa26 target, indicating that its low level of off-target effects do not come at the expense of on-target activity. These results suggest that various approaches might be tried to reduce off-target mutations in further studies. Additionally, the off-target mutations detected in this study might not be found in the clinic because of differences between the human and mouse genomes. Moreover, it is noteworthy that there were no definite morphological changes in the retinal pigment epithelium at 7 months after the subretinal injection, suggesting that the off-target mutations do not exert significant harmful effects (**Fig. 4D**).

In conclusion, we provide a new, CRISPR/Cas9-based approach for treating LCA. To our knowledge, no previous reports have shown *in vivo* HDR-mediated correction in animal models of ophthalmologic diseases. Our permanent therapeutic genome editing approach could be used alone, or together with gene therapy or protein therapy, to treat LCA.

Materials and Methods

Cell culture and transfection

MEFs were maintained in DMEM supplemented with 4.5 g/L glucose, 4 mM glutamine, 1 mM sodium pyruvate, 10% fetal bovine serum, 100 units/ml penicillin, and 100 mg/ml streptomycin. RNPs and 120-mer ssODN were transfected using Neon® Transfection following the manufacturer's procedures (Life Technologies). Briefly, 2.5 x 10^5 cells were mixed with materials for transfection were subjected to electrical shock using 10-μl tips on the Neon system for 30 ms at 1350 V for 1 pulse. Five days after transfection, the cells were harvested, and genomic DNA was extracted using a DNeasy Blood & Tissue kit (Qiagen). For transfections of HEK293 cells, cells were seeded at 2 x 10^5 cell/well into 24-well plates the day before transfection. 1 μg of plasmids encoding human optimized SpCas9 and sgRNA were mixed with 2 μl of lipofectamine 2000 (Invitrogen) in 200 μl of Opti-MEM, left for 20 min, and then added to cells that had reached 70% confluence in 500 μl of DMEM. After incubation for overnight, the medium was replaced with 500 μl of fresh medium, and genomic DNA was extracted after 5 days of transfection.

Animals

Eight-week-old male C57BL/6 mice and mating pairs of *rd12* mice (stock no. 005379, The Jackson Laboratory) were purchased from Central Laboratory Animal and maintained under a 12-hour dark-light cycle. *rd12* mice were mated with each other to produce offspring with a homozygous mutation in the *Rpe65* gene. All animal experiments were performed following guidelines from the Association for Research in Vision and Ophthalmology statement for the use of animals in ophthalmic and vision research and approved by Institutional Animal Care and Use Committees of both Seoul National University and Seoul National University Hospital.

Targeted deep sequencing

To quantify indel frequency, on-target and off-target regions were amplified by PCR from genomic DNA extracted from transfected cells, retina, or RPE using the primer sets summarized in TableS2. To quantify HDR frequencies, PCRs were first performed from genomic DNA (50 ng) using primers outside of the *Rpe65*-homology arm, after which

products were further amplified to generate amplicons for deep sequencing. The produced amplicons were barcoded during subsequent PCR with Illumina TrueSeq adaptors. The products were purified with PCR purification kit (Geneall), and then were pooled in equimolar ratio. The final libraries were paired-end sequenced using Illumina Miseq platform according to the manufacturer's protocol. Indel frequencies were quantified using Cas-Analyzer (www.rgenome.net) (*31*). Quantification of specific patterns such as in-frame- or out of frame-indels, 1-codon-deletions and precise HDR were determined by manual counting.

In silico identification of off-target sites

Potential off-target sites were identified using an *in silico* tool, Cas-OFFinder (*32*). Mouse genomic sites containing up to 3 bp mismatches were considered as off-target sites, and further confirmed by targeted deep sequencing using the primers shown in table S3.

In vitro cleavage of genomic DNA and Digenome-seq

Genomic DNA was purified from the retina of *rd12* mice with a DNeasy Tissue kit (Qiagen) according to the manufacturer's instructions. Genomic DNA (8 μg) was incubated with purified Cas9 protein (100 nM) and an sgRNA (300 nM) in a reaction volume of 400 μL for 8 h at 37°C in a buffer (100 mM NaCl, 40 mM Tris-HCl, 10 mM MgCl2, and 100 μg/ml BSA, pH 7.9). Digested genomic DNA was purified again with a DNeasy Tissue kit (Qiagen) after RNase A (50 μg/ml) was added to remove sgRNA. To check targeted *in vitro* DNA cleavage, digested genomic DNA was mixed with 2× Sybr Green Master Mix and analyzed by real-time quantitative PCR (qPCR) using forward primer 5'- GGACATTCTACATATGAATCCAGG-3' and reverse primer 5'-TAACATTCTCAGGTGGCTGTGCAA-3'. The fraction of target sites that were cleaved was measured using the comparative CT method (*33*).

For Digenome-seq, genomic DNA (1 μg) was sonicated to produce fragments in the 400- to 500-bp range using the Covaris system (Life Technologies) and blunt-ended using End Repair Mix (Thermo Fischer). Fragmented DNA was ligated with adapters to produce libraries, which were then subjected to whole-genome sequencing (WGS) using a HiSeq X Ten Sequencer (Illumina) at Macrogen. WGS was performed at a sequencing depth of 30–40× and the DNA cleavage score was calculated using a previously published scoring system (*34*).

AAV vector construction and virus production

Sequences of the EFS promoter and human optimized SpCas9 with a nuclear localization signal, HA-tag, and bovine growth hormone poly-A tail were synthesized and subcloned into an AAV2 inverted terminal repeat (ITR)-based plasmid using NotI restriction sites. For the other AAV vector, sequences of the U6 promoter, TS4 sgRNA, and *Rpe65* donor were also synthesized and subcloned into the AAV2 ITR-based plasmid using the same restriction sites. In the *Rpe65* donor sequences, 5 nucleotides were substituted without causing codon changes to prevent possible TS4 sgRNA-mediated cleavage and to precisely distinguish knocked-in sequences from endogenous genomic sequences. Recombinant AAV particles were produced using a helper adenovirus-free packaging system. Briefly, HEK293 cells were co-transfected with pAAV-ITR-EFS-SpCas9 or pAAV-ITR-TS4^{rd12}-sgRNA-*Rpe65* donor, AAV9-capsid plasmid, and helper plasmid.

After 3 days of transfection, the cells were lysed and the virus particles were purified by iodixanol gradient ultracentrifugation and concentrated to obtain titers greater than 10^{13} vg/ml.

Subretinal injection of AAV

After deep anesthesia, AAV9-SpCas9 and AAV9-TS4 sgRNA-*Rpe65*-donor (a total of $2x10^{10}$ vg or $2x10^{11}$ vg in 1 μl PBS) were mixed and injected into the subretinal space of the mouse eye through the vitreous cavity using a customized Nanofil syringe with a 33 G blunt needle (World Precision Instrument) under an operating microscope (Leica), as previously described (*35*).

Quantitative PCR for AAV genome detection in tissues

Quantitative PCR to determine the AAV genome copy number was performed using genomic DNA extracted from the retina or RPE. After measuring the genomic DNA concentration using a Quantus fluorometer together with the Quantifluor Dye system (Promega), 50 ng of genomic DNA was subjected to quantitative PCR analysis using an AAVpro titration kit (Takara). Thermocycling conditions were as follows: 95°C, 2 min followed by 35 cycles of 95°C, 5 sec; 60°C, 30 sec. The number of AAV genome copies was calculated against a standard curve. The number of diploid mouse cells was calculated using a conversion factor of ~1.6×10^4 diploid cells per 100 μg genomic DNA.

Electroretinography

Mice were dark-adapted for over 16 hours. After deep anesthesia, pupils were dilated with an eye drop containing phenylephrine hydrochloride (5 mg/ml) and tropicamide (5 mg/ml). Full-field electroretinography was performed using the universal testing and electrophysiologic system 2000 (UTAS E-2000, LKC Technologies). The scotopic responses were recorded with a flash of 0 dB at a gain of 2 k utilizing a notch filter at 60 Hz and were bandpass filtered between 0.1 and 1500 Hz. The amplitudes of the a-wave were measured from the baseline to the lowest negative-going voltage, whereas peak b-wave amplitudes were estimated from the trough of the a-wave to the highest peak of the positive b-wave.

Immunofluorescence (paraffin sections)

At 6 weeks after AAV-mediated delivery of SpCas9 and TS4 sgRNA-*Rpe65*-donor, paraffin blocks were prepared from enucleated eyes. Thin sections were immunostained with anti-HA antibody (1:1,000; cat. no. 3F10, Roche) and anti-Rpe65 antibody (1:1,000; cat. no. sc-73616, Santa Cruz), followed by treatment with Alexa Fluor 488 or 594 IgG (1:500; Thermo Fisher). Nuclear staining was performed using 4’,6-diamidino-2-phenylindole dihydrochloride (Sigma). The slides then were observed under a fluorescence microscope (Leica).

Quantitative real-time PCR

Total RNA was isolated using TRI Reagent (Molecular Research Center) from RPE cells of *rd12* mice at 7 months after AAV-mediated delivery of SpCas9 and TS4 sgRNA-*Rpe65*-donor. cDNAs were prepared with a High Capacity RNA-to-cDNA Kit (Thermo

Fisher). Real-time PCR was performed with the StepOnePlus Real-Time PCR System (Thermo Fisher) using TaqMan® Fast Advanced Master Mix (Thermo Fisher) with Gene Expression Assays (Thermo Fisher) for gene expression analyses. Product IDs of Gene Expression Assays for genes are as follows: for *Rpe65*, Mm00504133_m1; for *Gapdh*, Mm99999915_g1; and for *Rn18s*, Mm03928990_g1. The relative expression levels of the *Rpe65* gene were normalized to those of *Gapdh* and *Rn18s*. All procedures were performed in accordance with MIQE guidelines.

Histologic evaluation

At 7 months after AAV-mediated delivery of SpCas9 and TS4 sgRNA-*Rpe65*-donor, paraffin blocks were prepared from enucleated eyes. Thin sections were then prepared for H&E staining.

Immunofluorescence (whole mount preparation of RPE-choroid-scleral complexes)

At 7 months after AAV-mediated delivery of SpCas9 and TS4 sgRNA-*Rpe65*-donor, RPE-choroid-scleral complexes were prepared from enucleated eyes. Then, the complexes were immunostained with anti-ZO-1 antibody (5 μg/mL; cat. no. 61-7300, Thermo Fisher), followed by treatment with Alexa Fluor 594 IgG (1:500; Thermo Fisher). Nuclear staining was performed using 4’,6-diamidino-2-phenylindole dihydrochloride (Sigma). The slides then were observed under a fluorescence microscope (Leica).

Statistical analysis

All group results are expressed as mean ± SEM, if not stated otherwise. Statistical significance as compared to untreated controls is denoted with * ($P < 0.05$), ** ($P < 0.01$), *** ($P < 0.001$) in the figures and figure legends. Statistical analyses were performed using Graph Pad PRISM 5 and the specific tests are mentioned in the figure legends.

H2: Supplementary Materials

Fig. S1. Screening of sgRNAs targeting the *Rpe65* gene in *rd12* MEFs.
Fig. S2. Delivered AAV copies between retina and RPE.
Fig. S3. Analysis of human *RPE65* editing.
Fig. S4. Electroretinographic responses to bright stimuli (0 dB) after dark adaptation from normal C57BL/6 and *rd12* mice at 6 weeks after the injection (n = 4).
Fig. S5. Electroretinographic responses to dim stimuli (-25 dB) after dark adaptation from normal C57BL/6 and *rd12* mice at 6 weeks after the injection.
Fig. S6. Analysis of TS4 sgRNA off-target effects.
Fig. S7. Comparison of off target frequency between wild type SpCas9 and SniperCas9.
Table S1. Summary of predictions at the target site with sgRNA by the inDelphi approach.
Table S2. Active off-target sites.
Table S3. Primers used in this study.

References and Notes

1. A. V. Cideciyan, Leber congenital amaurosis due to RPE65 mutations and its treatment with gene therapy. *Prog. Retin. Eye Res.* **29**, 398-427 (2010).
2. A. I. den Hollander, R. Roepman, R. K. Koenekoop, F. P. Cremers, Leber congenital amaurosis: genes, proteins and disease mechanisms. *Prog. Retin. Eye Res.* **27**, 391-419 (2008).
3. J. W. Bainbridge, A. J. Smith, S. S. Barker, S. Robbie, R. Henderson, K. Balaggan, A. Viswanathan, G. E. Holder, A. Stockman, N. Tyler, S. Petersen-Jones, S. S. Bhattacharya, A. J. Thrasher, F. W. Fitzke, B. J. Carter, G. S. Rubin, A. T. Moore, R. R. Ali, Effect of gene therapy on visual function in Leber's congenital amaurosis. *N. Engl. J. Med.* **358**, 2231-2239 (2008).
4. A. M. Maguire, F. Simonelli, E. A. Pierce, E. N. Pugh, Jr., F. Mingozzi, J. Bennicelli, S. Banfi, K. A. Marshall, F. Testa, E. M. Surace, S. Rossi, A. Lyubarsky, V. R. Arruda, B. Konkle, E. Stone, J. Sun, J. Jacobs, L. Dell'Osso, R. Hertle, J. X. Ma, T. M. Redmond, X. Zhu, B. Hauck, O. Zelenaia, K. S. Shindler, M. G. Maguire, J. F. Wright, N. J. Volpe, J. W. McDonnell, A. Auricchio, K. A. High, J. Bennett, Safety and efficacy of gene transfer for Leber's congenital amaurosis. *N. Engl. J. Med.* **358**, 2240-2248 (2008).
5. W. W. Hauswirth, T. S. Aleman, S. Kaushal, A. V. Cideciyan, S. B. Schwartz, L. Wang, T. J. Conlon, S. L. Boye, T. R. Flotte, B. J. Byrne, S. G. Jacobson, Treatment of leber congenital amaurosis due to RPE65 mutations by ocular subretinal injection of adeno-associated virus gene vector: short-term results of a phase I trial. *Hum. Gene Ther.* **19**, 979-990 (2008).
6. G. M. Acland, G. D. Aguirre, J. Ray, Q. Zhang, T. S. Aleman, A. V. Cideciyan, S. E. Pearce-Kelling, V. Anand, Y. Zeng, A. M. Maguire, S. G. Jacobson, W. W. Hauswirth, J. Bennett, Gene therapy restores vision in a canine model of childhood blindness. *Nat. Genet.* **28**, 92-95 (2001).
7. K. Narfstrom, M. L. Katz, R. Bragadottir, M. Seeliger, A. Boulanger, T. M. Redmond, L. Caro, C. M. Lai, P. E. Rakoczy, Functional and structural recovery of the retina after gene therapy in the RPE65 null mutation dog. *Invest. Ophthalmol. Vis. Sci.* **44**, 1663-1672 (2003).
8. N. S. Dejneka, E. M. Surace, T. S. Aleman, A. V. Cideciyan, A. Lyubarsky, A. Savchenko, T. M. Redmond, W. Tang, Z. Wei, T. S. Rex, E. Glover, A. M. Maguire, E. N. Pugh, Jr., S. G. Jacobson, J. Bennett, In utero gene therapy rescues vision in a murine model of congenital blindness. *Mol. Ther.* **9**, 182-188 (2004).
9. J. Bennicelli, J. F. Wright, A. Komaromy, J. B. Jacobs, B. Hauck, O. Zelenaia, F. Mingozzi, D. Hui, D. Chung, T. S. Rex, Z. Wei, G. Qu, S. Zhou, C. Zeiss, V. R. Arruda, G. M. Acland, L. F. Dell'Osso, K. A. High, A. M. Maguire, J. Bennett, Reversal of blindness in animal models

of leber congenital amaurosis using optimized AAV2-mediated gene transfer. *Mol. Ther.* **16**, 458-465 (2008).
10. E. A. Pierce, J. Bennett, The Status of RPE65 Gene Therapy Trials: Safety and Efficacy. *Cold Spring Harb. Perspect. Med.* **5**, a017285 (2015).
11. S. W. Cho, S. Kim, J. M. Kim, J. S. Kim, Targeted genome engineering in human cells with the Cas9 RNA-guided endonuclease. *Nat. Biotechnol.* **31**, 230-232 (2013).
12. P. Mali, L. Yang, K. M. Esvelt, J. Aach, M. Guell, J. E. DiCarlo, J. E. Norville, G. M. Church, RNA-guided human genome engineering via Cas9. *Science* **339**, 823-826 (2013).
13. J. A. Doudna, E. Charpentier, Genome editing. The new frontier of genome engineering with CRISPR-Cas9. *Science* **346**, 1258096 (2014).
14.H. Kim, J. S. Kim, A guide to genome engineering with programmable nucleases. *Nat. Rev. Genet.* **15**, 321-334 (2014).
15. J. D. Sander, J. K. Joung, CRISPR-Cas systems for editing, regulating and targeting genomes. *Nat. Biotechnol.* **32**, 347-355 (2014).
16. H. Yin, W. Xue, S. Chen, R. L. Bogorad, E. Benedetti, M. Grompe, V. Koteliansky, P. A. Sharp, T. Jacks, D. G. Anderson, Genome editing with Cas9 in adult mice corrects a disease mutation and phenotype. *Nat. Biotechnol.* **32**, 551-553 (2014).
17. H. Yin, C. Q. Song, J. R. Dorkin, L. J. Zhu, Y. Li, Q. Wu, A. Park, J. Yang, S. Suresh, A. Bizhanova, A. Gupta, M. F. Bolukbasi, S. Walsh, R. L. Bogorad, G. Gao, Z. Weng, Y. Dong, V. Koteliansky, S. A. Wolfe, R. Langer, W. Xue, D. G. Anderson, Therapeutic genome editing by combined viral and non-viral delivery of CRISPR system components in vivo. *Nat. Biotechnol.* **34**, 328-333 (2016).
18.Y. Yang, L. Wang, P. Bell, D. McMenamin, Z. He, J. White, H. Yu, C. Xu, H. Morizono, K. Musunuru, M. L. Batshaw, J. M. Wilson, A dual AAV system enables the Cas9-mediated correction of a metabolic liver disease in newborn mice. *Nat. Biotechnol.* **34**, 334-338 (2016).
19. M. W. Shen, M. Arbab, J. Y. Hsu, D. Worstell, S. J. Culbertson, O. Krabbe, C. A. Cassa, D. R. Liu, D. K. Gifford, R. I. Sherwood, Predictable and precise template-free CRISPR editing of pathogenic variants. *Nature* **563**, 646-651 (2018).
20. J. J. Pang, B. Chang, N. L. Hawes, R. E. Hurd, M. T. Davisson, J. Li, S. M. Noorwez, R. Malhotra, J. H. McDowell, S. Kaushal, W. W. Hauswirth, S. Nusinowitz, D. A. Thompson, J. R. Heckenlively, Retinal degeneration 12 (rd12): a new, spontaneously arising mouse model for human Leber congenital amaurosis (LCA). *Mol. Vis.* **11**, 152-162 (2005).
21. D. Kim, S. Bae, J. Park, E. Kim, S. Kim, H. R. Yu, J. Hwang, J. I. Kim, J. S. Kim, Digenome-seq: genome-wide profiling of CRISPR-Cas9 off-target effects in human cells. *Nat. Methods* **12**, 237-243 (2015).
22. J. Nishiyama, T. Mikuni, R. Yasuda, Virus-Mediated Genome Editing via Homology-Directed Repair in Mitotic and Postmitotic Cells in Mammalian Brain. *Neuron* **96**, 755-768 e755 (2017).
23. N. E. Bengtsson, J. K. Hall, G. L. Odom, M. P. Phelps, C. R. Andrus, R. D. Hawkins, S. D. Hauschka, J. R. Chamberlain, J. S. Chamberlain, Muscle-specific CRISPR/Cas9 dystrophin gene editing ameliorates pathophysiology in a mouse model for Duchenne muscular dystrophy. *Nat. Commun.* **8**, 14454 (2017).
24. K. Suzuki, Y. Tsunekawa, R. Hernandez-Benitez, J. Wu, J. Zhu, E. J. Kim, F. Hatanaka, M. Yamamoto, T. Araoka, Z. Li, M. Kurita, T. Hishida, M. Li, E. Aizawa, S. Guo, S. Chen, A. Goebl, R. D. Soligalla, J. Qu, T. Jiang, X. Fu, M. Jafari, C. R. Esteban, W. T. Berggren, J. Lajara, E. Nunez-Delicado, P. Guillen, J. M. Campistol, F. Matsuzaki, G. H. Liu, P. Magistretti, K. Zhang, E. M. Callaway, K. Zhang, J. C. Belmonte, In vivo genome editing via CRISPR/Cas9 mediated homology-independent targeted integration. *Nature* **540**, 144-149 (2016).

25. J. W. Bainbridge, M. S. Mehat, V. Sundaram, S. J. Robbie, S. E. Barker, C. Ripamonti, A. Georgiadis, F. M. Mowat, S. G. Beattie, P. J. Gardner, K. L. Feathers, V. A. Luong, S. Yzer, K. Balaggan, A. Viswanathan, T. J. de Ravel, I. Casteels, G. E. Holder, N. Tyler, F. W. Fitzke, R. G. Weleber, M. Nardini, A. T. Moore, D. A. Thompson, S. M. Petersen-Jones, M. Michaelides, L. I. van den Born, A. Stockman, A. J. Smith, G. Rubin, R. R. Ali, Long-term effect of gene therapy on Leber's congenital amaurosis. *N. Engl. J. Med.* **372**, 1887-1897 (2015).
26. S. G. Jacobson, A. V. Cideciyan, A. J. Roman, A. Sumaroka, S. B. Schwartz, E. Heon, W. W. Hauswirth, Improvement and decline in vision with gene therapy in childhood blindness. *N. Engl. J. Med.* **372**, 1920-1926 (2015).
27. J. S. Chen, Y. S. Dagdas, B. P. Kleinstiver, M. M. Welch, A. A. Sousa, L. B. Harrington, S. H. Sternberg, J. K. Joung, A. Yildiz, J. A. Doudna, Enhanced proofreading governs CRISPR-Cas9 targeting accuracy. *Nature* **550**, 407-410 (2017).
28. J. K. Lee, E. Jeong, J. Lee, M. Jung, E. Shin, Y. H. Kim, K. Lee, I. Jung, D. Kim, S. Kim, J. S. Kim, Directed evolution of CRISPR-Cas9 to increase its specificity. *Nat. Commun.* **9**, 3048 (2018).
29. G. X. Ruan, E. Barry, D. Yu, M. Lukason, S. H. Cheng, A. Scaria, CRISPR/Cas9-Mediated Genome Editing as a Therapeutic Approach for Leber Congenital Amaurosis 10. *Mol. Ther.* **25**, 331-341 (2017).
30. B. Zetsche, S. E. Volz, F. Zhang, A split-Cas9 architecture for inducible genome editing and transcription modulation. *Nat. Biotechnol.* **33**, 139-142 (2015).
31. J. Park, K. Lim, J. S. Kim, S. Bae, Cas-analyzer: an online tool for assessing genome editing results using NGS data. *Bioinformatics* **33**, 286-288 (2017).
32. S. Bae, J. Park, J. S. Kim, Cas-OFFinder: a fast and versatile algorithm that searches for potential off-target sites of Cas9 RNA-guided endonucleases. *Bioinformatics* **30**, 1473-1475 (2014).
33. T. D. Schmittgen, K. J. Livak, Analyzing real-time PCR data by the comparative C(T) method. *Nat. Protoc.* **3**, 1101-1108 (2008).
34. D. Kim, S. Kim, S. Kim, J. Park, J. S. Kim, Genome-wide target specificities of CRISPR-Cas9 nucleases revealed by multiplex Digenome-seq. *Genome Res* **26**, 406-415 (2016).
35. S. W. Park, J. H. Kim, W. J. Park, J. H. Kim, Limbal approach-subretinal injection of viral vectors for gene therapy in mice retinal pigment epithelium. *J. Vis. Exp.*, e53030 (2015).

Acknowledgments

We thank Dr. Lee JK (ToolGen, Inc.) for kind gift of SniperCas9-expressing vector.

Funding: This research was supported by Ministry of Food and Drug Safety (**17172MFDS213**), the National Research Foundation of Korea (NRF) funded by the Korea government (MSIT) (**2017M3A9B4061406**), the Bio & Medical Technology Development Program of the National Research Foundation funded by the Korean government, MSIP (**NRF-2015M3A9E6028949** and **2017M3A9B4062654** to Je.H.K.), the Creative Materials Discovery Program through the National Research Foundation of Korea (NRF) funded by Ministry of Science and ICT (**2018M3D1A1058826** to Je.H.K), Development of Platform Technology for Innovative Medical Measurements funded by Korea Research Institute of Standards and Science (**KRISS-2018-GP2018-0018** to Je.H.K.), and the Basic Science Research Program through the National Research Foundation of Korea (NRF) funded by the Ministry of Education (**2017R1A6A3A04004741** to D.H.J.).

Author contributions: D.H.J. drafted the manuscript and performed/analyzed animal experiments. D.W.S. drafted the manuscript and performed/analyzed genome editing experiments. C.S.C. and S.W.P. performed animal experiments. U.G.K. and K.J.L. performed genome editing experiments. K.L. and Ji.H.K. edited the manuscript. D.K. performed Digenome-seq. S.K. and J.-S.K. revised the manuscript. Je.H.K. and J.M.L. designed the study and revised the manuscript.

Competing interests: D.W.S., U.G.K, K.J.L., S.K., and J.M.L are employed by ToolGen. D.W.S, U.G.K, J.M.L, D.H.J, and Je.H.K. have filed patent applications based on this work. J.-S.K. is a co-founder and shareholder of ToolGen, Inc. The remaining authors declare no competing financial interests.

Data and materials availability: All data needed to evaluate the conclusions in the paper are present in the paper and/or the Supplementary Materials. Additional data related to this paper are available from authors upon request.

Figures and Tables

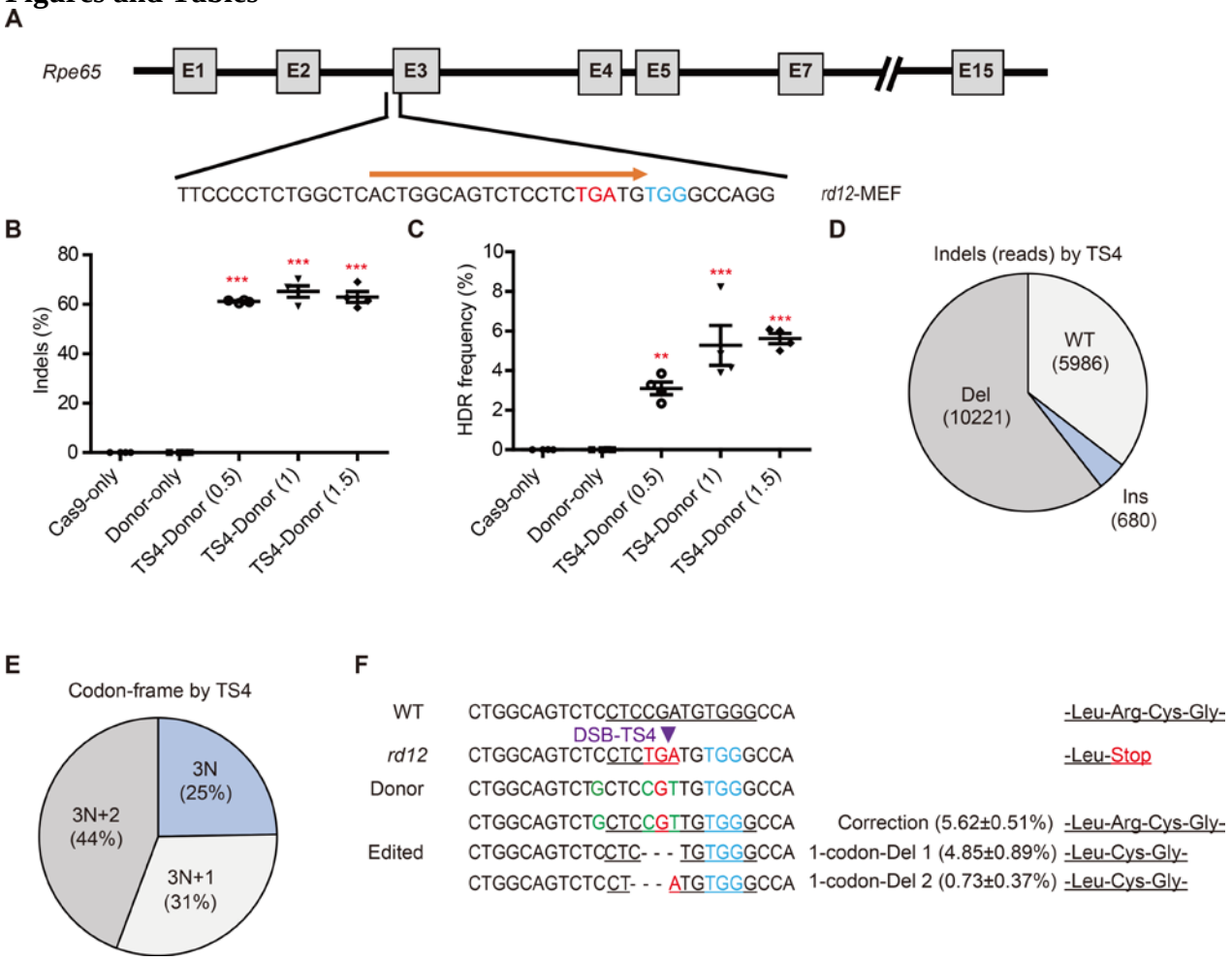

Figure 1. Genome editing of *Rpe65* by CRISPR/Cas9 *in vitro*. (**A**) A schematic drawing of *Rpe65* in *rd12* MEF. Red text, sequence of the premature stop codon; orange arrow, TS4 sgRNA target sequence; blue text, protospacer adjacent motif (PAM). (**B**) TS4 sgRNA-induced indel frequencies measured by targeted deep sequencing (n = 4). ssODN dose (μg) are indicated in parenthesis. (**C**) Correction frequencies in the *rd12* mutation measured by targeted deep sequencing (n = 4). (**D**) Mean values of the number of deep sequencing reads in different categories show the pattern of indels induced by the TS4 sgRNA (n = 4). Of the total reads, about 61% contain deletions. Ins, insertion; Del, deletion; WT, wild type. (**E**) Mean percent values of different types of in-frame and out-of-frame indels induced by the TS4 sgRNA (n = 4). 3N, one codon; 3N+1, one codon+1 nucleotide; 3N+2, one codon+2 nucleotides. (**F**) Nucleotide sequences showing types of editing induced by the TS4 sgRNA and 1.5μg of ssODN in *rd12* MEF (n =4). Violet triangle, position of the DSB induced by the TS4 sgRNA; red text, sequences of the stop codon in *rd12* MEF; blue text: PAM sequences; green text: synonymous mutations in the donor template; underlined sequences, nucleotides encompassing the premature stop codon and their corresponding amino acid sequences. Error bars indicate SEM. **, $P < 0.01$; ***, $P < 0.001$ by Kruskal-Wallis test with Dunn's multiple comparison test.

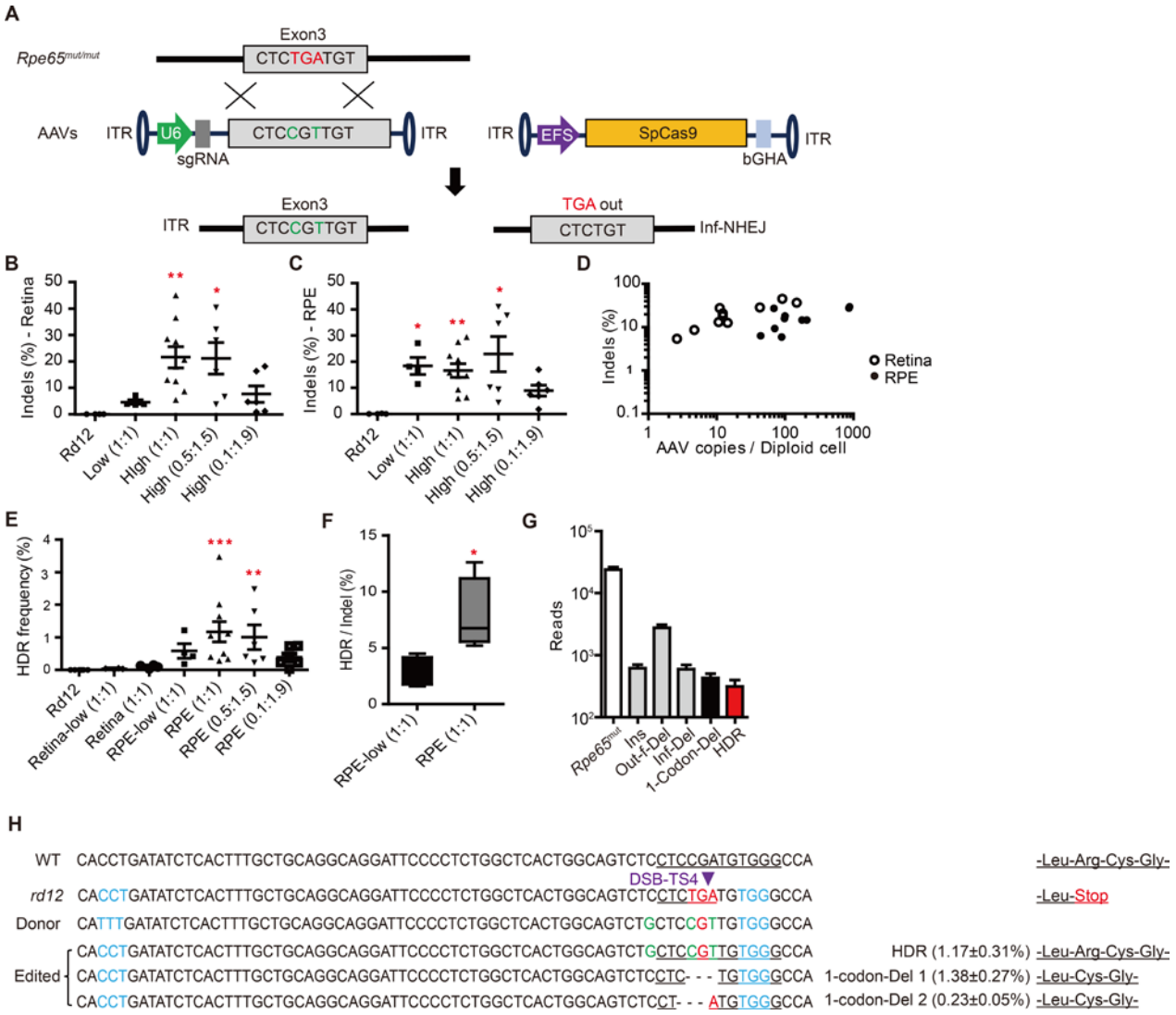

H

```
WT      CACCTGATATCTCACTTTGCTGCAGGCAGGATTCCCCTCTGGCTCACTGGCAGTCTCCTCCGATGTGGGCCA                    -Leu-Arg-Cys-Gly-
                                                  DSB-TS4
rd12    CACCTGATATCTCACTTTGCTGCAGGCAGGATTCCCCTCTGGCTCACTGGCAGTCTCCTCTGATGTGGGCCA                    -Leu-Stop
Donor   CATTTGATATCTCACTTTGCTGCAGGCAGGATTCCCCTCTGGCTCACTGGCAGTCTGCTCCGTTGTGGGCCA
Edited  CACCTGATATCTCACTTTGCTGCAGGCAGGATTCCCCTCTGGCTCACTGGCAGTCTGCTCCGTTGTGGGCCA  HDR (1.17±0.31%)  -Leu-Arg-Cys-Gly-
        CACCTGATATCTCACTTTGCTGCAGGCAGGATTCCCCTCTGGCTCACTGGCAGTCTCCTC- - - TGTGGGCCA  1-codon-Del 1 (1.38±0.27%)  -Leu-Cys-Gly-
        CACCTGATATCTCACTTTGCTGCAGGCAGGATTCCCCTCTGGCTCACTGGCAGTCTCCT- - - ATGTGGGCCA  1-codon-Del 2 (0.23±0.05%)  -Leu-Cys-Gly-
```

Figure 2. HDR-mediated genome editing induced by CRISPR/Cas9 in the retina and RPE of *rd12* mice. (**A**) A schematic drawing of the dual AAV strategy for CRISPR/Cas9-mediated therapeutic correction of the nonsense mutation in *Rpe65* in *rd12* mice. The premature stop codon in *Rpe65* (red text) is generated by a C-to-T mutation in exon 3. The U6 and EFS promoters in the AAV vector were used to express the sgRNA together with the donor template and SpCas9, respectively. Green text, synonymous mutations in the donor template. Therapeutic gene correction could be derived from HDR-mediated precise correction (HDR) or in-frame NHEJ (Inf-NHEJ). (**B,C**) Indel frequencies measured by targeted deep sequencing in the retina (**B**) and RPE (**C**) of *rd12* mice at 4 weeks post injection of high dose (a total of $2x10^{11}$ vg/eye) and low dose (a total of $2x10^{10}$ vg/eye) AAV. SpCas9 to TS4 sgRNA-*Rpe65*-donor ratios are indicated in parentheses. (**D**) Correlation between the indel frequency and AAV copy number per diploid cell (n=10). A high dose of 1:1 ratio of SpCas9 and TS4 sgRNA-*Rpe65*-donor was injected subretinally. (**E**) Frequencies of therapeutic HDR at the site of the C-to-T mutation in the retina and RPE of *rd12* mice at 4 weeks post injection. (**F**) Ratio of HDR to indel frequencies. A high or low dose of SpCas9 and TS4 sgRNA-*Rpe65*-donor at a 1:1 ratio was injected subretinally (n = 4). (**G**) Mean values of the number of deep sequencing reads including insertions, deletions, or HDR in AAV-treated RPE (n = 10). A high dose of 1:1 ratio of SpCas9 and TS4 sgRNA-*Rpe65*-donor was injected subretinally. *Rpe65*^{mut}, non edited; Ins, insertion; Out-f-Del, out

of frame deletion; Inf-Del, in-frame deletion. (**H**) Nucleotide sequences showing the *Rpe65* donor template and changes induced by the TS4 sgRNA in AAV-treated RPE (n = 10). A high dose of 1:1 ratio of SpCas9 and TS4 sgRNA-*Rpe65*-donor was injected subretinally. Violet triangle, position of the DSB induced by the TS4 sgRNA; red text, sequences corresponding to the premature stop codon in *rd12* mice; blue text: PAM sequences; green text: synonymous mutations in the donor template; underlined sequences, nucleotides encompassing the premature stop codon and their corresponding amino acid sequences. *, $P < 0.05$; **, $P < 0.01$; ***, $P < 0.001$ by Kruskal-Wallis test with Dunn's multiple comparison test (B,C,E) and Mann-Whitney U-test (F).

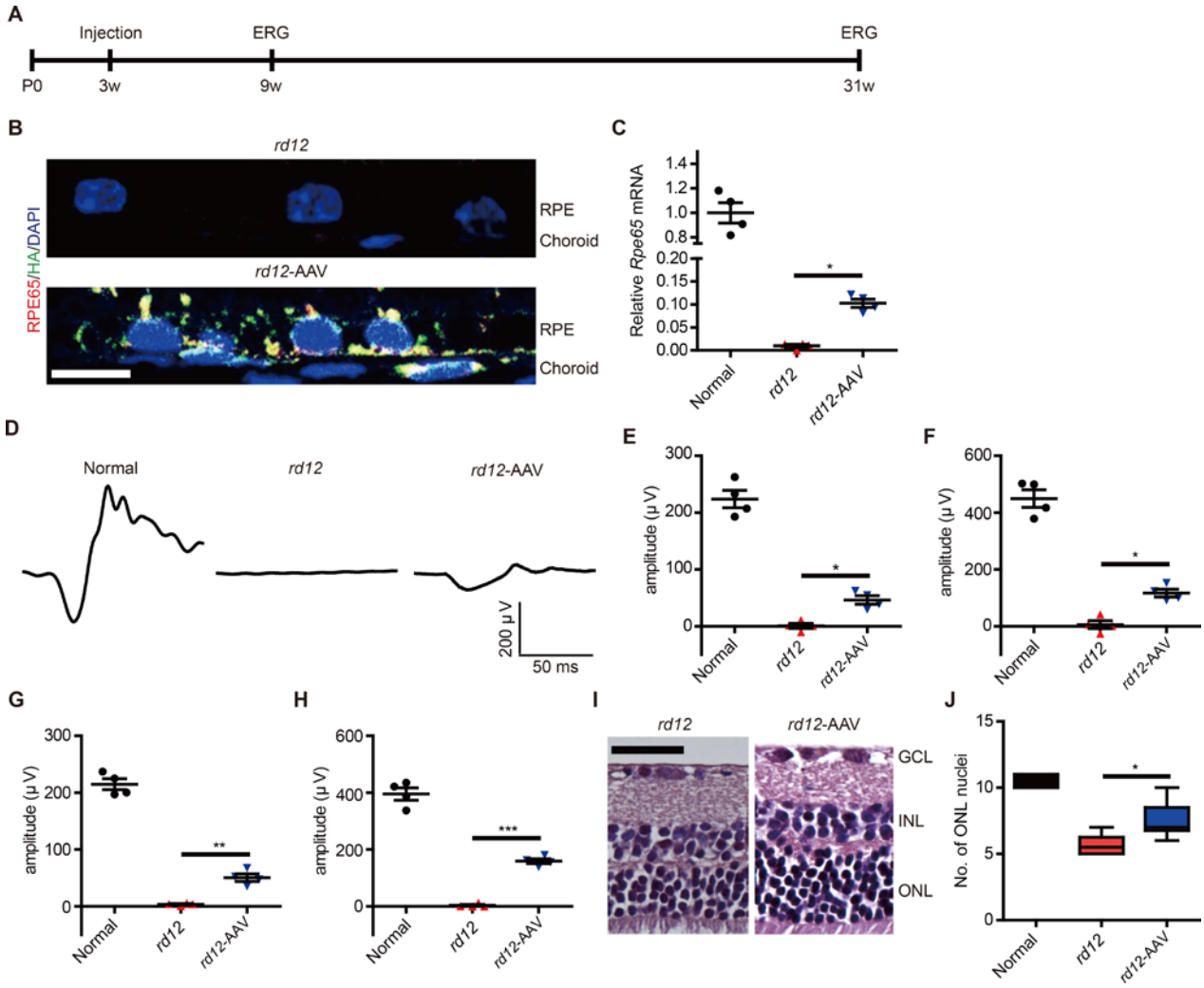

Figure 3. Therapeutic effects of HDR-mediated correction of the *Rpe65* gene in *rd12* mice. (**A**) Overview of animal experiments. Time points for subretinal injection and electroretinography are indicated. P0, postnatal day 0; ERG, electroretinography; w, weeks. (**B**) RPE65 protein expression in the RPE layer of *rd12* mice at 6 weeks after the injection. Scale bar, 10 μm. (**C**) The relative expression of *Rpe65* mRNA in the RPE cells of *rd12* mice at 7 months after the injection (n = 4). (**D**) Representative electroretinographic responses to bright stimuli (0 dB) after dark adaptation from normal C57BL/6 and *rd12* mice at 6 weeks after the injection. (**E-H**) Amplitudes of electroretinographic responses to bright stimuli (0 dB) after dark adaptation (n = 4). (**E,G**) Amplitudes of the a-wave at 0 dB at 6 weeks (**E**) and 7 months (**G**) after the injection. (**F,H**) Amplitudes of the b-wave at 0 dB at 6 weeks (**F**) and 7 months (**H**) after the injection. (**I**) Representative H&E images of retinal tissues from *rd12* mice at 7 months after the injection. Scale bar, 20 μm. (**J**) The number of layers of outer nuclear layer nuclei in *rd12* mice at 7 months after the injection (n = 4). Normal, C57BL/6; *rd12*, *rd12* mice without treatment; *rd12-AAV*, *rd12* mice treated with subretinal injection of a high dose of 1:1 ratio of SpCas9 and TS4 sgRNA-*Rpe65*-donor. *, $P < 0.05$; **, $P < 0.01$; ***, $P < 0.001$ by Kruskal-Wallis test with Dunn's multiple comparison test.

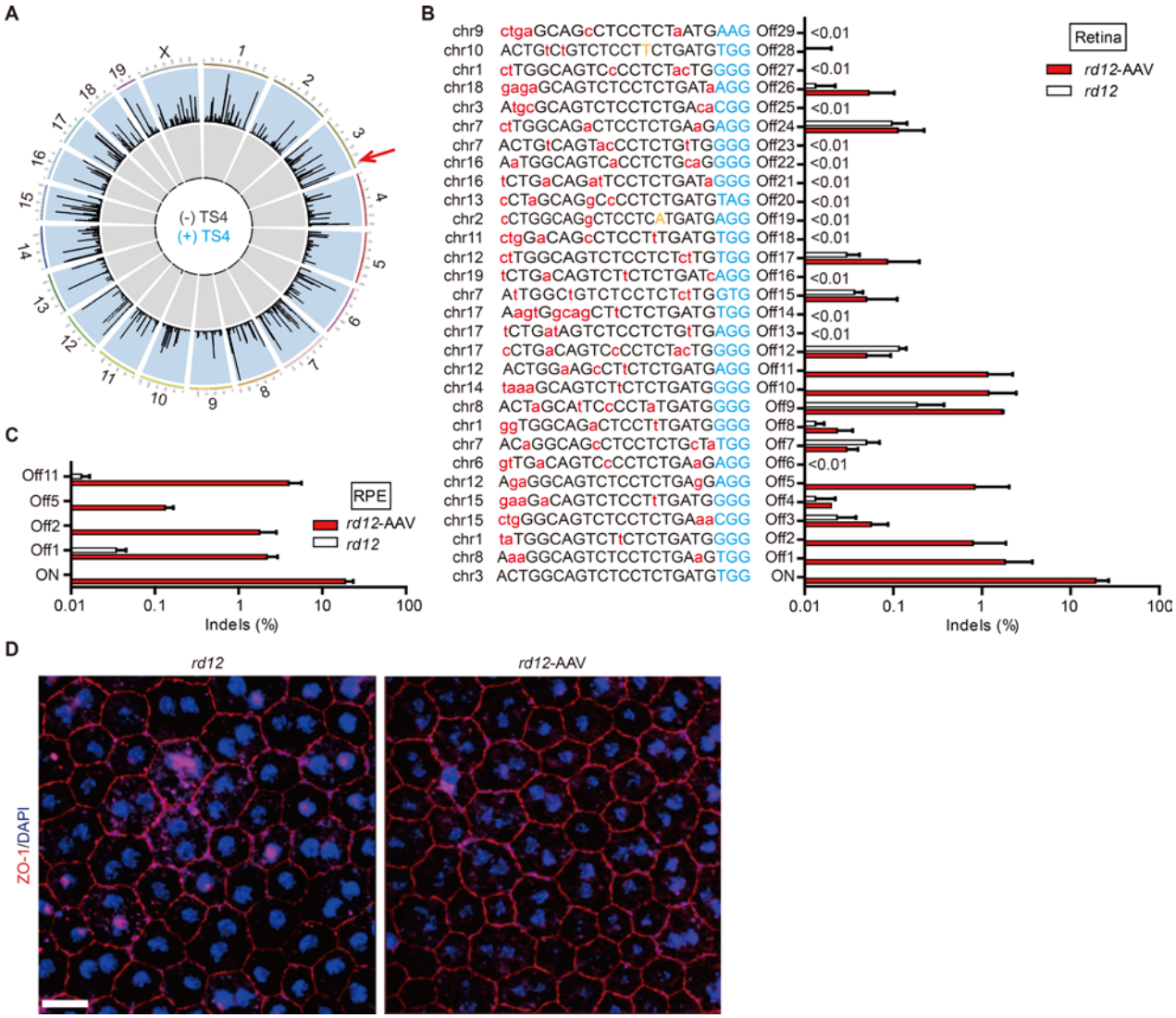

Figure 4. Analysis of potential off-target sites. (**A**) Genome-wide Circos plot showing *in vitro* cleavage sites in the *rd12* mouse genome in the absence (gray) or in the presence (blue) of TS4 sgRNA. On-target cleavage is indicated by the red arrow. (**B**) Targeted deep sequencing results for the top 29 Digenome-seq candidates in AAV-treated retina (n = 3). Nucleotides in red and orange indicate sequences that are mismatched relative to the on-target site, and nucleotides in blue indicate PAM sequences. (**C**) Re-analysis of the active off-targets by targeted deep sequencing in AAV-treated RPE (n = 3). (**D**) Representative whole mount of RPE tissues from *rd12* mice at 7 months post-treatment with or without the dual AAV system encoding SpCas9 and the donor template. Scale bar, 10 μm.